Transportation Research Part C 126 (2021) 103043

Contents lists available at ScienceDirect

Transportation Research Part C

journal homepage: www.elsevier.com/locate/trc

Robust perimeter control with cordon queues and heterogeneous transfer flows

Ye Li [a], Mehmet Yildirimoglu [b], Mohsen Ramezani [a,*]

[a] The University of Sydney, School of Civil Engineering, Australia
[b] The University of Queensland, School of Civil Engineering, Australia

ARTICLE INFO

Keywords:
Network fundamental diagram
Gating
Variable structure control
Robust control
Congestion management

ABSTRACT

Accumulation-based Macroscopic Fundamental Diagram (MFD) model is widely employed to design perimeter control methods to improve traffic operation in urban networks. While the accumulation-based MFD assumes a low-scatter, non-linear relationship between region production and accumulation, the outflow relationship in formulating dynamics of multi-region networks requires simplifying assumptions. The existing perimeter control methods are grounded on accumulation-based MFD models where the number of transferring vehicles is approximated by the ratio of the instantaneous number of vehicles based on their destinations. Moreover, perimeter control may lead to more vehicles queuing at the region boundary (i.e. cordon queues) which add local impediments on traveling vehicles and impact the accuracy of well-defined MFDs. To address these shortcomings under time-varying conditions, this paper develops a robust perimeter control method based on the Sliding Mode Control to minimize total travel time in the entire network. To test the performance of the proposed control method, a trip-based MFD model is developed that accounts for cordon queues and various trip lengths of individual travelers. In this paper, two-region accumulation-based and trip-based MFD models are compared through numerical experiments. The results pinpoint the proposed robust perimeter control method can effectively alleviate congestion and improve network efficiency during traffic rush hours.

1. Introduction

Excessive traffic congestion has become a quotidian problem in urban cities with the growing transport demand. To alleviate congestion and improve the network efficiency, several management approaches for large-scale transport systems have been developed, such as perimeter flow control (e.g. Geroliminis et al., 2013; Fu et al., 2020; Ingole et al., 2020), congestion pricing (e.g. Zheng and Geroliminis, 2020), and coordinated ramp metering (e.g. Han et al., 2020). Perimeter flow control was found to be an effective approach to manipulate traffic flows between regions to maintain vehicle accumulation in regions under a predefined value (i.e. critical accumulation). The perimeter control is implemented using coordination among traffic signals installed at boundaries between the regions to regulate the rate of transferring vehicles from one region to another to prevent hypercongestion.

Recently, sizable research studied perimeter control approaches, see Haddad and Shraiber (2014), Ramezani et al. (2015), Yang et al. (2018), Lei et al. (2019), Haddad and Mirkin (2020) among others. These approaches utilize accumulation-based MFD model

* Corresponding author.
E-mail address: mohsen.ramezani@sydney.edu.au (M. Ramezani).

https://doi.org/10.1016/j.trc.2021.103043
Received 19 August 2020; Received in revised form 11 February 2021; Accepted 11 February 2021
Available online 12 March 2021

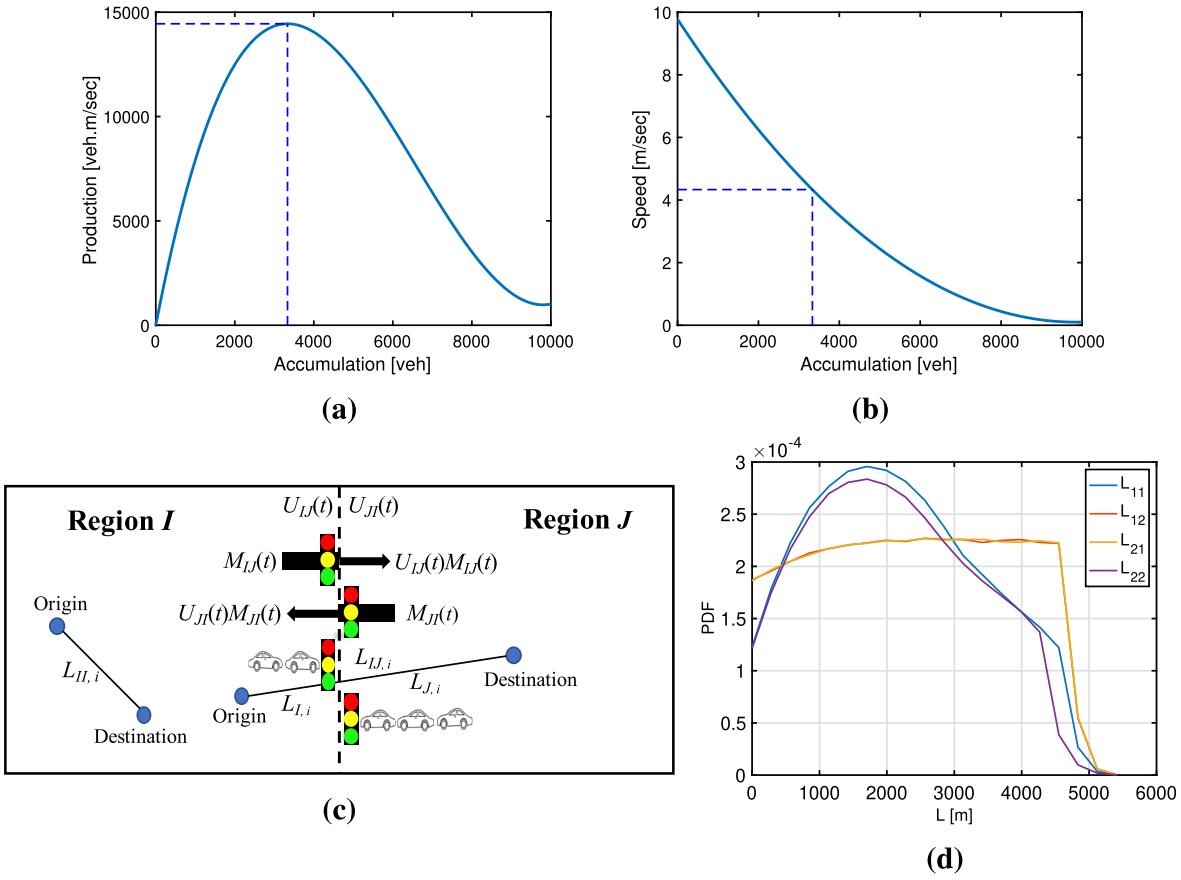

Fig. 1. (a) Production MFD used in Accumulation-based MFD models, (b) Speed MFD used in Trip-based MFD models, (c) the two-region network structure with cordon queues, and (d) different trip length distributions (sampled offline and used in the trip-based MFD model).

grounded on a parsimonious, low-scattered, and non-linear relationship between vehicle accumulation [veh] and production [veh·m/s] of the network, see Fig. 1(a). While the congestion is homogeneously distributed in the network, the aggregated accumulation-based MFD can be employed to model the traffic dynamics (see Geroliminis and Daganzo, 2008). The MFD model was originally proposed by Godfrey (1969). The theoretical concepts of MFD were first established in Daganzo (2007), and its existence was demonstrated in Geroliminis and Daganzo (2008) utilizing field data from downtown Yokohama, Japan. The MFD dynamic foundation of a single region was established in Daganzo (2007), where the evolution of traveling vehicle accumulation is modeled by tracking the incoming traffic demand and endogenous traffic outflow. In networks without uniformly distributed vehicle densities, MFD exhibits a hysteresis loop. To cope with this issue, one recognized approach is to partition a heterogeneously congested network into multiple regions with homogeneous congestion distributions (see Saeedmanesh and Geroliminis, 2016; Saedi et al., 2020). The partitioning further enables to manipulate the transferring flows between regions by the traffic signals located at region boundaries. The perimeter flow control is a coordinated action among these traffic signals.

Perimeter control grounded on accumulation-based MFD has been introduced for single-region (e.g. Daganzo, 2007; Keyvan-Ekbatani et al., 2012) and multi-region networks (e.g. Ramezani et al., 2015; Kouvelas et al., 2017; Csikós et al., 2017; Yang et al., 2018, 2019). The perimeter control settles at the peripheries between regions to manipulate the percentages of transfer flows. However, restricting transferring vehicles might result in queuing vehicles at region boundaries. The queuing vehicles affect the traffic flow dynamics and consequently might influence the outflow of the region and accuracy of well-defined MFD (Haddad, 2017). So the cordon queue impacts should be carefully addressed. Ni and Cassidy (2020) proposed to model time-varying queue impacts on network production by re-scaling MFD at any time step, where the MFD is scaled downward or upward respectively when the cordon queue size grows or shrinks. In this paper, we develop a robust perimeter controller that tackles the effect of cordon queues on congestion propagation.

Many studies have constructed perimeter control framework using techniques such as Bang-Bang control (see Daganzo, 2007; Aalipour et al., 2018), Proportional-Integral (PI) control (see Keyvan-Ekbatani et al., 2015; Mohajerpoor et al., 2019; Ingole et al., 2020), Model Predictive Control (MPC) (see Geroliminis et al., 2013; Fu et al., 2017; Kim et al., 2019), and Linear Quadratic Regulator (LQR) (see Haddad and Shraiber, 2014; Haddad, 2015). The model-based perimeter controllers for multi-region networks require an assumption for the transferring flows in the accumulation-based MFD model. In most cases, the ratio between the internal and external

outflows is assumed to be equal to the ratio of the instantaneous number of vehicles based on their destinations, (e.g. in Ramezani et al., 2015; Zhong et al., 2018; Yang et al., 2019). This assumption imposes modeling inaccuracy and would lessen the performance of model-based controllers, specifically the ones based on model predictions such as MPC.

This paper proposes a robust perimeter controller based on Sliding Mode Control (SMC) method to address the inherent mismatch between the traffic flow model (i.e. MFD) and real world traffic dynamics. This is crucial because MFD is inherently a spatially and temporally aggregated model and neglects several (micro) aspects of traffic. Specifically, the proposed SMC perimeter controller is designed to tackle the following issues in multi-region MFD modeling; (i) the effect of cordon queues on congestion heterogeneity and MFD and (ii) the split ratio between internal and external outflows. The SMC is a variable structure control method that accounts for uncertainties in modeling formulation and measurements. The SMC enables discontinuous and nonlinear control gains to stabilize the system by manipulating the state of the system to predefined (sliding) surfaces in finite time and maintain the states on them thereafter (e.g. Aalipour et al., 2017; Bichiou et al., 2020).

One notable characteristic of employing accumulation-based MFD model is the numerical tractability that offers optimization and control opportunities. To this end, several studies assume an average trip length representing all vehicles within the network (e.g. Loder et al., 2019; Huang et al., 2020). Recent studies highlight the effect of various trip lengths on accumulation-based MFD model (Mariotte et al., 2017; Batista and Leclercq, 2019). In particular, Mariotte et al. (2020a) demonstrated that the calibration of trip lengths is crucial for accuracy of the MFD models. To take into consideration the different trip lengths of vehicles, the trip-based MFD was first proposed by Arnott (2013), and applied in later research such as Lamotte and Geroliminis (2018), Yildirimoglu and Ramezani (2020), Jin (2020). Trip-based MFD assumes a well-defined relation between vehicle accumulation and mean speed of the network, see Fig. 1(b). Mariotte et al. (2017) employed a one-region network to compare the accumulation-based MFD and trip-based MFD models, and pinpointed incoherence during transient phases. When the system operates under steady state, the two models are consistent with each other (i.e. analogous accumulation evolution), while in the loading and unloading phases, they exhibit substantial differences. Similar results are observed in multi-region networks (Mariotte and Leclercq, 2019). A multi-region trip-based MFD model requires more complicated states to describe traffic dynamics, e.g. vehicle accumulations towards internal or external destinations and their related trip lengths. This paper introduces a two-region trip-based model that considers cordon queues to be employed as a testbed to investigate the proposed robust perimeter controller.

The contributions of this paper are threefold: (i) designing a real-time, robust perimeter control based on Sliding Mode Control (SMC) method to tackle the inherent uncertainties in multi-region accumulation-based MFD model, (ii) developing a two-region trip-based MFD model considering cordon queue dynamics, and (iii) testing the proposed robust perimeter control on the trip-based MFD model to investigate its effectiveness. In this paper, it is assumed the urban network is divided into two regions. The perimeter control regulates the flows between the two regions, and vehicles waiting to cross the boundary represent the cordon queues, as delineated in Fig. 1(c). An accumulation-based MFD model with uncertain parameters is established to develop a robust traffic control method. The controller is applied to the trip-based MFD model that accounts for the effects of cordon queues which are considered as one aggregated queue consistent with the physics of MFD. To further investigate the SMC efficiency, an improved Bang-Bang controller is introduced for comparison.

The remainder of this paper is organized as follows. Section 2 introduces the two-region accumulation-based MFD model and the trip-based MFD model accounting for cordon queues. Section 3 develops an SMC scheme grounded on the accumulation-based MFD model to minimize the network total time spent. Also, an improved Bang-Bang controller is introduced for comparison. Section 4 employs numerical experiments to investigate the two models as well as to evaluate the controller performance, under two disparate demand profiles. Finally, in Section 5, the paper closes with the summary and future research directions.

2. Macroscopic traffic modeling

In this section, the two-region trip-based and accumulation-based MFD models are introduced. The former is considered as the plant that accounts for the perimeter control, cordon queues, and heterogeneous transfer flows. The trip-based MFD model, which is the more detailed model, tracks the number of vehicles grouped as queued and traveling with internal or external destinations. On the other hand, the proposed parsimonious accumulation-based MFD model is employed to derive the robust perimeter control based on SMC while neglecting the dynamics of cordon queues.

2.1. Trip-based MFD model: accounting for perimeter control and cordon queue dynamics

The trip-based MFD model is a disaggregated yet city-wide model that takes into account individual travel details such as trip length and departure time (see Mariotte et al., 2017). In this section, we introduce the event-based implementation of the trip-based MFD model (Mariotte et al., 2017; Yildirimoglu and Ramezani, 2020) for a network divided into two regions with perimeter control and considering the cordon queue dynamics. The events contain departure (from the origin) and arrival (to the destination), joining and leaving cordon queues for vehicles with origin in one region and destination in another region, and changes in perimeter control values. Every event directly affects the accumulations in regions and hence regions mean speeds.

The network is assumed to be partitioned into two regions, denoted by Region $I, J = \{1, 2\}$. The exogenous travel demands entering the network are associated to different trip lengths and departure times (from their origins). Let $N_{IJ}^{Q}(t)$ [veh] denote the number of queuing vehicles at the boundary in Region I with the destination in Region J at time t. Note that the queuing vehicles only consist of vehicles traveling between regions, and the vehicles suffer the queuing process at most once during their whole trips. The traveling

accumulations in Region $I, N_I^{\mathrm{T}}(t)$ [veh], includes the number of traveling vehicles heading to internal and external destinations, that is $N_I^{\mathrm{T}}(t) = N_{II}^{\mathrm{T}}(t) + N_{IJ}^{\mathrm{T}}(t)$. As a result, the total number of vehicles in Region I at time t is, $N_I(t) = N_I^{\mathrm{T}}(t) + N_{IJ}^{\mathrm{Q}}(t)$. We consider the Production-MFD of Region $I, P_I(N_I(t))$ [veh·m/s], is re-scaled with respect to the number of traveling and queuing vehicles at time t (Ni and Cassidy, 2020), as shown in the following,

$$\widetilde{P}_I\left(N_I^{\mathrm{T}}(t), N_{IJ}^{\mathrm{Q}}(t)\right) = \left(1 - \frac{N_{IJ}^{\mathrm{Q}}(t)}{N_I^{\mathrm{jam}}}\right) \cdot P_I\left(\frac{N_I^{\mathrm{T}}(t)}{1 - N_I^{\mathrm{Q}}(t)/N_I^{\mathrm{jam}}}\right) = a \cdot \left(N_I^{\mathrm{T}}(t)\right)^3 \left(\frac{N_I^{\mathrm{jam}}}{N_I^{\mathrm{jam}} - N_{IJ}^{\mathrm{Q}}(t)}\right)^2 + b \cdot \left(N_I^{\mathrm{T}}(t)\right)^2 \left(\frac{N_I^{\mathrm{jam}}}{N_I^{\mathrm{jam}} - N_{IJ}^{\mathrm{Q}}(t)}\right) + c \cdot N_I^{\mathrm{T}}(t), \quad (1)$$

where N_I^{jam} [veh] is the jam accumulation of Region $I, \widetilde{P}_I(N_I^{\mathrm{T}}(t), N_{IJ}^{\mathrm{Q}}(t))$ is the re-scaled Production-MFD, and a, b, c are the estimated parameters for the upper-envelope Production-MFD, i.e. $P_I(N_I(t)) = a \cdot (N_I(t))^3 + b \cdot (N_I(t))^2 + c \cdot N_I(t)$.

The re-scaled mean speed of Region I at time $t, \widetilde{V}_I(N_I^{\mathrm{T}}(t), N_{IJ}^{\mathrm{Q}}(t))$ [m/s], used in trip-based MFD model[1] based on the traveling and queued vehicle accumulations is

$$\widetilde{V}_I\left(N_I^{\mathrm{T}}\left(t\right), N_{IJ}^{\mathrm{Q}}\left(t\right)\right) = \frac{\widetilde{P}_I\left(N_I^{\mathrm{T}}\left(t\right), N_{IJ}^{\mathrm{Q}}\left(t\right)\right)}{N_I^{\mathrm{T}}(t)}. \quad (2)$$

This indicates that the speed changes when the number of traveling and/or queued vehicles changes. Based on the network speed, the traveled distance between events is calculated, and the vehicles exit the network once their assigned trip lengths are completed. The model gets updated when an event occurs, i.e. the time instance when a vehicle enters or exits a region, or joins or leaves a cordon queue, or perimeter control values changes. In which case, the entire time duration might be unevenly separated between events. The fundamental principle of individual vehicle i's trip length towards an internal destination, i.e., $L_{II,i}$ [m], should satisfy,

$$L_{II,i} = \int_{t_i^{\mathrm{dep}}}^{t_i^{\mathrm{arr}}} \widetilde{V}_I\left(N_I^{\mathrm{T}}\left(t\right), N_{IJ}^{\mathrm{Q}}\left(t\right)\right) \mathrm{d}t. \quad (3)$$

And for vehicle i's trip length towards an external destination, i.e., $L_{IJ,i}$ [m], should satisfy,

$$L_{IJ,i} = \int_{t_i^{\mathrm{dep}}}^{t_i^{\mathrm{Q}_I}} \widetilde{V}_I\left(N_I^{\mathrm{T}}(t), N_{IJ}^{\mathrm{Q}}(t)\right) \mathrm{d}t + \int_{t_i^{\mathrm{LQ}_I}}^{t_i^{\mathrm{arr}}} \widetilde{V}_J\left(N_J^{\mathrm{T}}(t), N_{JI}^{\mathrm{Q}}(t)\right) \mathrm{d}t \quad (4)$$

where t_i^{dep} and t_i^{arr} [s] are departure and arrival times of vehicle $i, t_i^{\mathrm{Q}_I}$ and $t_i^{\mathrm{LQ}_I}$ [s] are the time that vehicle i joins and leaves the cordon queue in Region I, and $\widetilde{V}_I(N_I^{\mathrm{T}}(t), N_{IJ}^{\mathrm{Q}}(t))$ and $\widetilde{V}_J(N_J^{\mathrm{T}}(t), N_{JI}^{\mathrm{Q}}(t))$ [m/s] are the re-scaled regional mean speed of Region I and J at time t, respectively. Note that $t_i^{\mathrm{Q}_I}, t_i^{\mathrm{LQ}_I}$, and t_i^{arr} are function of t_i^{dep}, see Eq. (6) and Eq. (7). Also, it should be noted that for vehicles traveling between regions, i.e. Eq. (4), $L_{IJ,i}$ contains two terms associated with travel distance in Region $I, L_{I,i}$, and in Region $J, L_{J,i}$ [m], such that $L_{IJ,i} = L_{I,i} + L_{J,i}$, as shown in Fig. 1(c). Eq. (3) and Eq. (4) aim to realize the traveled distance of vehicle i, while the trip lengths and departure times are model inputs for both internal and external trips. Without loss of generality, we assume the travel lengths are the Euclidean distance between the origins and the destinations considering a plane network. With sampling numerous pairs of origins and destinations in both regions, the trip length distributions of L_{11}, L_{12}, L_{21}, and L_{22} are sampled offline, shown in Fig. 1(d). In the trip-based MFD model, the trip length for each vehicle is *randomly* assigned from the *predefined distributions* at the beginning of their trip.

The trip-based MFD model is served as the plant to replicate the actual number of transferring flows, such that the outputs of the model are the arrival times of vehicles with internal and external trips, and the time when the vehicles join and leave cordon queues. Note that we consider the cordon queues as one aggregated queue, one in each region, consistent with the physics of MFD; and the effect of growing or shrinking cordon queue size is captured in re-scaled Speed-MFD. Since the perimeter control restricts transfer flows between the regions, the model should take into account the entry flow capacity of regions. This is a joint function of the border capacity between the regions and the available space in the destination region. Similar with Ramezani et al. (2015), we consider the entry flow capacity $C_{IJ}(N_J(t))$ [veh/s] as a piecewise two-segment function; first a constant value reflecting border capacity value ($\overline{\mathrm{C}}_{IJ}$), followed by a decreasing positive function of accumulation of Region J:

$$C_{IJ}(N_J(t)) = \begin{cases} \overline{\mathrm{C}}_{IJ} & \text{if } 0 \leqslant N_J(t) < \alpha \cdot N_J^{\mathrm{jam}}, \\ \dfrac{\overline{\mathrm{C}}_{IJ}}{(1-\alpha)}\left(1 - \dfrac{N_J(t)}{N_J^{\mathrm{jam}}}\right) & \text{if } \alpha \cdot N_J^{\mathrm{jam}} \leqslant N_J(t) \leqslant N_J^{\mathrm{jam}}, \end{cases} \quad (5)$$

where $0 < \alpha < 1$ defines the deflection accumulation in Region J when the entry flow capacity starts to decline; and $\overline{\mathrm{C}}_{IJ}$ [veh/s] is the

[1] The difference between $\widetilde{P}_I(N_I^{\mathrm{T}}(t), N_{IJ}^{\mathrm{Q}}(t))/N_I^{\mathrm{T}}(t)$ and $\widetilde{P}_I(N_I^{\mathrm{T}}(t), N_{IJ}^{\mathrm{Q}}(t))/N_I(t)$ is that the former represents the mean speed of traveling vehicles and the latter represents the mean speed of all vehicles in Region I. The proposed trip-based model tracks the travel distance of vehicles; this only constitutes traveling vehicles, thus the mean speed of traveling vehicles should be used.

boundary capacity between Regions I and J that denotes the possible maximum number of queued vehicles that can pass the boundary. $\overline{C}_{IJ}$ can be estimated in real life as an aggregation of the capacity of the streets upstream of perimeter traffic signals. Boundary capacity is the maximum number of vehicles per unit time that can pass through the intersections under disparate roadway, traffic, and signalization conditions, while the capacity can be maximized through several methods (see Amirgholy et al., 2020). Note that, other entry flow and exit flow models (e.g. Mariotte and Leclercq, 2019; Mariotte et al., 2020b) can be readily integrated within the two-region trip-based model while validation with real data is a research priority. Furthermore, the calibration of α is a challenging task especially in multi-region settings since it is needed to capture the complicated multi-path entry flow dynamics.

We define the time-varying remaining trip length as $L_{II,i}(t)$ and $L_{IJ,i}(t)$ [m]. They are updated at each time instance when a new event occurs such that if vehicle i travels inside Region I, $L_{II,i}(t') = L_{II,i}(t) - (t' - t) \cdot \widetilde{V}_I(N_I^{\mathrm{T}}(t), N_{IJ}^{\mathrm{Q}}(t))$, if vehicle i is in Region I and travels from Region I towards Region J, $L_{I,i}(t') = L_{I,i}(t) - (t' - t) \cdot \widetilde{V}_I(N_I^{\mathrm{T}}(t), N_{IJ}^{\mathrm{Q}}(t))$, and if vehicle i is in Region J and traveled from Region I towards Region J, $L_{J,i}(t') = L_{J,i}(t) - (t' - t) \cdot \widetilde{V}_J(N_J^{\mathrm{T}}(t), N_{JI}^{\mathrm{Q}}(t))$, where t [s] is the time of current event and t' [s] is the time of next event. Note that similar to the total travel distance $L_{IJ,i}$, the remaining trip length of vehicle i traveling between regions is $L_{IJ,i}(t) = L_{I,i}(t) + L_{J,i}(t)$. With this in mind, the estimation of arrival time of vehicle i at time t traveling with an internal destination in Region I is[2],

$$t_i^{\mathrm{arr}}(t) = t + \frac{L_{II,i}(t)}{\widetilde{V}_I(N_I^{\mathrm{T}}(t), N_{IJ}^{\mathrm{Q}}(t))}. \tag{6}$$

If vehicle i travels from Region I to Region J, the estimated join queue time, leave queue time, and arrival time are,

$$t_i^{\mathrm{Q}_I} = t + \frac{L_{I,i}(t)}{\widetilde{V}_I\left(N_I^{\mathrm{T}}\left(t\right), N_{IJ}^{\mathrm{Q}}\left(t\right)\right)} \tag{7a}$$

$$t_i^{\mathrm{LQ}_I} = t_i^{\mathrm{Q}_I} + \frac{N_{IJ}^{\mathrm{Q}}(t) + 1}{C_{IJ}(N_J(t)) \cdot U_{IJ}(t)} \tag{7b}$$

$$t_i^{\mathrm{arr}} = t_i^{\mathrm{LQ}_I} + \frac{L_{J,i}(t)}{\widetilde{V}_J\left(N_J^{\mathrm{T}}\left(t\right), N_{JI}^{\mathrm{Q}}\left(t\right)\right)} \tag{7c}$$

where $U_{IJ}(t)$ denotes the perimeter control manipulating the transfer flows from Region I to Region J at time t, and $0 \leqslant U_{\min} \leqslant U_{IJ}(t) \leqslant U_{\max} \leqslant 1$. Note that Eq. (6) and Eq. (7) are applied to all individual vehicles in the network after each event such that all potential event times are re-estimated and the next imminent event is identified. Eq. (7) are not only applied as potential estimates of event times but also employed for the vehicles already started their trips. Hence the current status of the vehicles (e.g. traveling or queuing), and their current locations (e.g. in Region I or Region J) should be taken into account. That is, if the size of cordon queue changes or in case the perimeter control value changes, then Eq. (7b) switches to, $t_i^{\mathrm{LQ}_I} = t + z_i^{\mathrm{Q}_I}(t)/(C_{IJ}(N_J(t)) \cdot U_{IJ}(t))$. Here, $z_i^{\mathrm{Q}_I}(t)$ is the position of vehicle i in the cordon queue in Region I at time t. Ultimately, when vehicle i passes the boundary and starts traveling in Region J, Eq. (7c) becomes, $t_i^{\mathrm{arr}} = t + L_{J,i}(t)/\widetilde{V}_J(N_J^{\mathrm{T}}(t), N_{JI}^{\mathrm{Q}}(t))$.

The pseudo-code of the two-region trip-based MFD model is detailed below. For the sake of brevity, region subscripts of $t_i^{\mathrm{Q}}, t_i^{\mathrm{LQ}}$, and t_i^{arr} are omitted.

Algorithm 1. Two-region trip-based MFD model pseudo-code

```
Initialize event_list=[]
Initialize previous_time = t_init

for All vehicles (i) do
    Add t_i^dep to event_list
    Determine the initial t_i^Q, t_i^LQ, t_i^arr based on Eq. (6) or Eq. (7) considering initial mean region speed
    Add t_i^Q, t_i^LQ, and t_i^arr to event_list
end for
Sort event_list based on event time

while there are events in the event_list do
    current_time ← the time of the first event in event_list
    for All current traveling vehicles in the network do
        if vehicle i destination is inside Region I then
            RL_II,i ← RL_II,i - Ṽ_I(N_I^T(t), N_IJ^Q(t))· (current_time - previous_time)
        else if vehicle i travels from Region I to J then
            if vehicle i currently in Region I then
```

(continued on next page)

[2] Accordingly, the estimated arrival time at the time of departure reads $t_i^{\mathrm{arr}}(t_i^{\mathrm{dep}}) = t_i^{\mathrm{dep}} + L_{II,i}/\widetilde{V}_I(N_I^{\mathrm{T}}(t_i^{\mathrm{dep}}), N_{IJ}^{\mathrm{Q}}(t_i^{\mathrm{dep}}))$.

(*continued*)

$RL_{I,i} \leftarrow RL_{I,i}$ - $\widetilde{V}_I(N_I^T(t), N_{IJ}^Q(t))$ · (current_time - previous_time)
else if vehicle i currently in Region J **then**
$RL_{J,i} \leftarrow RL_{J,i}$ - $\widetilde{V}_J(N_J^T(t), N_{JI}^Q(t))$· (current_time - previous_time)
end if
end if
end for
if The first event is vehicle departure **then**
if The vehicle departures in Region I **then**
$N_I^T(t) \leftarrow N_I^T(t)+1$
else if The vehicle departures in Region J **then**
$N_J^T(t) \leftarrow N_J^T(t)+1$
end if
else if The first event is vehicle arrival **then**
if The vehicle arrives from Region I **then**
$N_I^T(t) \leftarrow N_I^T(t)$-1
else if The vehicle arrives from Region J **then**
$N_J^T(t) \leftarrow N_J^T(t)$-1
end if
else if The first event is vehicle join cordon queue **then**
if The vehicle joins the cordon queue in Region I **then**
$N_{IJ}^Q(t) \leftarrow N_{IJ}^Q(t)+1$, $N_I^T(t) \leftarrow N_I^T(t)$-1
else if The vehicle joins the cordon queue in Region J **then**
$N_{JI}^Q(t) \leftarrow N_{JI}^Q(t)+1$, $N_J^T(t) \leftarrow N_J^T(t)$-1
end if
else if The first event is vehicle leave cordon queue **then**
if The vehicle leaves the cordon queue in Region I **then**
$N_{IJ}^Q(t) \leftarrow N_{IJ}^Q(t)$-1, $N_J^T(t) \leftarrow N_J^T(t)+1$
else if The vehicle leaves the cordon queue in Region J **then**
$N_{JI}^Q(t) \leftarrow N_{JI}^Q(t)$-1, $N_I^T(t) \leftarrow N_I^T(t)+1$
end if
else if The first event is a new perimeter control value **then**
update t_i^{LQ} and t_i^{arr} for all vehicles with respect to Eq. (6) and Eq. (7), considering current vehicle statuses and locations
end if
update $\widetilde{P}_I(N_I^T(t), N_{IJ}^Q(t))$ and $\widetilde{P}_J(N_J^T(t), N_{JI}^Q(t))$ using Eq. (1)
update $\widetilde{V}_I(N_I^T(t), N_{IJ}^Q(t))$ and $\widetilde{V}_J(N_J^T(t), N_{JI}^Q(t))$ using Eq. (2)
for all vehicles in the network **do**
update join queue time, leave queue time, and arrival time based on Eq. (6) and Eq. (7) with the new regional mean speed, $\widetilde{V}_I(N_I^T(t), N_{IJ}^Q(t))$ and $\widetilde{V}_J(N_J^T(t), N_{JI}^Q(t))$
end for
Remove the first event in the event_list
end while

Note that the trip-based MFD model terminates once all the vehicles exit the network. Note also that the trip-based MFD model is not necessarily a first in first out (FIFO) model since all vehicles in the network might travel with distinct trip lengths, see Yildirimoglu and Ramezani (2020).

2.2. Accumulation-based MFD model: accounting perimeter control and heterogeneous transfer flow

In this section, we present the two-region accumulation-based MFD model with perimeter control and a general (uncertain) representation of transfer flows. In majority of literature (e.g. Yildirimoglu et al., 2015; Ramezani and Nourinejad, 2018; Yildirimoglu et al., 2018; Sirmatel and Geroliminis, 2019), the accumulation-based MFD model did not differentiate between traveling and queued vehicles; while Haddad (2017) and Ni and Cassidy (2020) modeled these two groups of vehicles separately. Also, a FIFO-based exit function as in Paipuri and Leclercq (2020) may be utilized to estimate the number of queuing vehicles in accumulation-based MFD models. In this paper, we resort to employ the parsimonious accumulation-based MFD models with no differentiation between the traveling and queuing vehicles to simplify the controller design. However, the proposed trip-based MFD model considers traveling and queued vehicles to offer a more detailed picture of traffic dynamics in real networks with perimeter control. The time-varying vehicle accumulations in Region I and J are represented by $N_I(t)$ and $N_J(t)$ [veh], respectively. Vehicle accumulations in Region I bound for internal and external destinations are denoted by $N_{II}(t)$ and $N_{IJ}(t)$ [veh], such that $N_I(t) = N_{II}(t) + N_{IJ}(t)$. Furthermore, the accumulation fraction, $N_{IJ}(t)/N_I(t)$, is assumed to approximately model the transfer flow between Region I and Region J. This assumption is relaxed in this paper by introducing unknown time-varying (yet partially observable) parameters in the accumulation-based MFD model, $\theta(t)$. We define $0 \leqslant \theta_I(t) \leqslant 1$ corresponding to the internal part of the outflow of Region I (i.e. trips with internal destinations), and

$1-\theta_I(t)$ associated with the external part of the outflow of Region I (transfer flows, i.e. trips with external destinations).[3]

At the network level, the accumulation-based MFD considers 'Production-MFD' in Region $I, P_I(N_I(t))$ [veh·m/s], and assumes that the network outflow, $G_I(N_I(t)) = P_I(N_I(t))/L_I$, where L_I [m] denotes the average trip length in Region I. The exogenous travel demands are composed of Region I's demands heading to its neighbour Region $J, Q_{IJ}(t)$, and those towards destinations inside Region $I, Q_{II}(t)$ [veh/s]. The perimeter control located at the boundary between the two regions, $U_{IJ}(t)$ and $U_{JI}(t)$, manipulate transfer flows such that $0 \leqslant U_{\min} \leqslant U_{IJ}(t), U_{JI}(t) \leqslant U_{\max} \leqslant 1$. The presented accumulation-based MFD model does not consider cordon queue dynamics in order to simplify the controller design. With this choice, the perimeter flow controller does not require the number of queued vehicles and the re-scaled Production-MFD. Therefore, we adopted a robust control approach using SMC method to overcome this simplification in modeling. The accumulation conservation equations are as:

$$\frac{\mathrm{d}N_{II}(t)}{\mathrm{d}t} = Q_{II}\left(t\right) - \theta_I\left(t\right) \cdot \frac{P_I(N_I(t))}{L_{II}(t)} + \left(1-\theta_J\left(t\right)\right) \cdot U_{JI}\left(t\right) \cdot \frac{P_J(N_J(t))}{L_{JI}(t)} \tag{8a}$$

$$\frac{\mathrm{d}N_{IJ}(t)}{\mathrm{d}t} = Q_{IJ}\left(t\right) - \left(1-\theta_I\left(t\right)\right) \cdot U_{IJ}\left(t\right) \cdot \frac{P_I(N_I(t))}{L_{IJ}(t)} \tag{8b}$$

where $L_{II}(t)$ [m] is the average travel distance of vehicles with internal destinations, and $L_{IJ}(t)$ and $L_{JI}(t)$ [m] are the average travel distance of vehicles with external destinations. Eq. (8) associates the change in vehicles accumulations with the inflows and outflows inside a region or from one region to another. Note that the average trip lengths, $L_{II}(t)$ and $L_{IJ}(t)$, can be time-varying while for the sake of simplicity we adopt time-invariant values in the numerical tests.

It is worth mentioning that $\theta_I(t)$ is partially observed in real-time to a certain degree of accuracy by measuring the number of vehicles passing through the perimeter control intersections. However, in the accumulation-based MFD model, $\theta_I(t)$ is estimated as $N_{II}(t)/N_I(t)$, and it is more challenging to be predicted as it intrinsically required in MPC approaches. In addition, $\theta_I(t)$ is a source of uncertainty in modeling while SMC is robust to deal with unobservable variations in model variables, and hence a robust perimeter control based on SMC theory is applied that take into account uncertainties in the MFD model. Note that the proposed SMC perimeter controller is designed grounded on the accumulation-based MFD model while applied on the trip-based MFD model, such that $\theta(t)$ is not required in the proposed controller. From there, the consistency check of these two different models is necessary where the numerical experiments are presented in Section 4.1.

3. Controller design

3.1. Sliding mode control

Sliding Mode Control (SMC) is a robust control approach to provide a desired dynamic behavior regardless of uncertainties and disturbance in the model (see Slotine, 1984; Canale et al., 2008; Spurgeon, 2014). In this section, SMC is designed building on the accumulation-based MFD model in Eq. (8) to manipulate the system states reach predefined sliding surfaces and maintain on the surfaces thereafter (Bichiou et al., 2020). This paper applies a similar control framework as Aalipour et al. (2017).

We rearrange the state variables of the system as $X_1(t) = N_{11}(t) + N_{21}(t), X_2(t) = N_{12}(t), X_3(t) = N_{21}(t)$, and $X_4(t) = N_{12}(t) + N_{22}(t)$. The traffic dynamics of the two-region network with the new rearranged states are,

$$\dot{X}_1\left(t\right) = Q_{11}\left(t\right) + Q_{21}\left(t\right) - M_{11}^{\mathrm{X}}\left(t\right) \tag{9a}$$

$$\dot{X}_2\left(t\right) = Q_{12}\left(t\right) - M_{12}^{\mathrm{X}}\left(t\right) U_{12}\left(t\right) \tag{9b}$$

$$\dot{X}_3\left(t\right) = Q_{21}\left(t\right) - M_{21}^{\mathrm{X}}\left(t\right) U_{21}\left(t\right) \tag{9c}$$

$$\dot{X}_4\left(t\right) = Q_{22}\left(t\right) + Q_{12}\left(t\right) - M_{22}^{\mathrm{X}}\left(t\right) \tag{9d}$$

such that the external outflows and control signals are merely appeared in two traffic states (i.e. $X_2(t)$ and $X_3(t)$). The rearranged internal and external outflows are,

$$M_{11}^{\mathrm{X}}\left(t\right) = \theta_1\left(t\right) \cdot \frac{P_1(X_1(t) - X_3(t) + X_2(t))}{L_{11}(t)} \tag{10a}$$

$$M_{12}^{\mathrm{X}}\left(t\right) = \left(1-\theta_1\left(t\right)\right) \cdot \frac{P_1(X_1(t) - X_3(t) + X_2(t))}{L_{12}(t)} \tag{10b}$$

[3] $\theta_I(t)$ can be accurately enough estimated as $N_{II}(t)/N_I(t)$ in steady state conditions in MFD models.

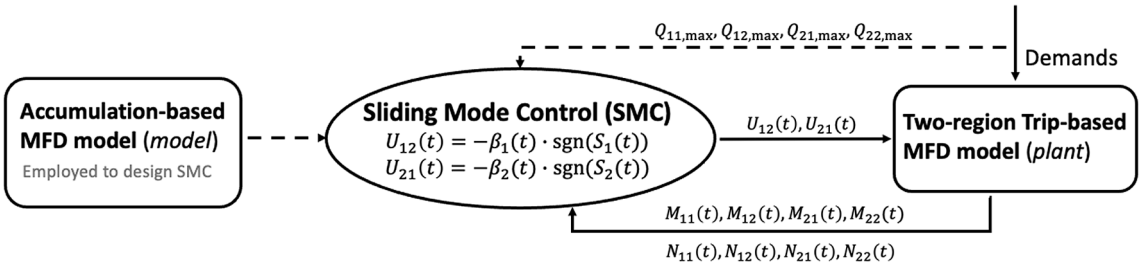

Fig. 2. The control architecture of the proposed perimeter control method based on SMC. The accumulation-based MFD model is employed to design the controller. The trip-based MFD model is considered as the plant. The solid arrows represent online procedures.

$$M_{21}^{X}\left(t\right) = \left(1-\theta_2\left(t\right)\right) \cdot \frac{P_2(X_4(t) - X_2(t) + X_3(t))}{L_{21}(t)} \tag{10c}$$

$$M_{22}^{X}\left(t\right) = \theta_2\left(t\right) \cdot \frac{P_2(X_4(t) - X_2(t) + X_3(t))}{L_{22}(t)}. \tag{10d}$$

Note that the rearranged outflows hold akin calculation logic with the outflows in Eq. (8), e.g. $M_{12}(t) = M_{12}^{X}(t) = (1-\theta_1(t)) \cdot P_1(N_1(t))/L_{12}(t)$.

The sliding surfaces are considered as, $S_1(t) = X_4(t) - k_1 \cdot X_2(t)$ and $S_2(t) = X_1(t) - k_2 \cdot X_3(t)$, where positive parameters k_1 and k_2 are designed to ensure stability. The evolution of the states of the system over time are forced towards the sliding surfaces $S_1(t) = 0$ and $S_2(t) = 0$. The derivatives of sliding surfaces are,

$$\dot{S}_1\left(t\right) = Q_{22}\left(t\right) + \left(1-k_1\right)Q_{12}\left(t\right) - M_{22}^{X}\left(t\right) + k_1 U_{12}\left(t\right)M_{12}^{X}\left(t\right) \tag{11a}$$

$$\dot{S}_2\left(t\right) = Q_{11}\left(t\right) + \left(1-k_2\right)Q_{21}\left(t\right) - M_{11}^{X}\left(t\right) + k_2 U_{21}\left(t\right)M_{21}^{X}\left(t\right). \tag{11b}$$

To analyze the stability, we define the following inequalities,

$$\rho_1\left(t\right) \geqslant \left|\frac{Q_{22}\left(t\right) + \left(1-k_1\right)Q_{12}\left(t\right) - M_{22}^{X}\left(t\right)}{k_1 M_{12}^{X}\left(t\right)}\right| \tag{12a}$$

$$\rho_2\left(t\right) \geqslant \left|\frac{Q_{11}\left(t\right) + \left(1-k_2\right)Q_{21}\left(t\right) - M_{11}^{X}\left(t\right)}{k_2 M_{21}^{X}\left(t\right)}\right|, \tag{12b}$$

such that the above inequalities can be guaranteed by defining the variables $\rho_1(t)$ and $\rho_2(t)$ as,

$$\rho_1\left(t\right) = \frac{Q_{22,max} + \left(k_1 - 1\right)Q_{12,max} + M_{22}^{X}\left(t\right)}{k_1 M_{12}^{X}\left(t\right)} \tag{13a}$$

$$\rho_2\left(t\right) = \frac{Q_{11,max} + \left(k_2 - 1\right)Q_{21,max} + M_{11}^{X}\left(t\right)}{k_2 M_{21}^{X}\left(t\right)}, \tag{13b}$$

where $Q_{11,max}, Q_{12,max}, Q_{21,max}$, and $Q_{22,max}$ [veh/s] are the maximum values of $Q_{11}(t), Q_{12}(t), Q_{21}(t)$, and $Q_{22}(t)$, respectively. The Lyapunov candidate function is considered as $v(t) = (S_1(t)^2 + S_2(t)^2)/2$, to compel the trajectories moving towards sliding surfaces and to ensure the surfaces are stable. The derivative of $v(t)$ is,

$$\begin{aligned} \dot{v}(t) &= S_1(t)\dot{S}_1(t) + S_2(t)\dot{S}_2(t) \\ &= S_1(t)\left(Q_{22}(t) + (1-k_1)Q_{12}(t) - M_{22}^{X}(t) + k_1 M_{12}^{X}(t)U_{12}(t)\right) + S_2(t)\left(Q_{11}(t) + (1-k_2)Q_{21}(t) - M_{11}^{X}(t) + k_2 M_{21}^{X}(t)U_{21}(t)\right) \\ &\leqslant |S_1(t)|\rho_1(t)k_1 M_{12}^{X}(t) + U_{12}(t)S_1(t)k_1 M_{12}^{X}(t) + |S_2(t)|\rho_2(t)k_2 M_{21}^{X}(t) + U_{21}(t)S_2(t)k_2 M_{21}^{X}(t). \end{aligned} \tag{14}$$

To satisfy precedent conditions, we define the discontinuous perimeter control inputs as,

$$U_{12}(t) = -\beta_1(t) \cdot \mathrm{sgn}(S_1(t)) \tag{15a}$$

$$U_{21}(t) = -\beta_2(t) \cdot \mathrm{sgn}(S_2(t)) \tag{15b}$$

where $\beta_1(t) > \rho_1(t) + \beta_0$ and $\beta_2(t) > \rho_2(t) + \beta_0$, and β_0 is a positive and relatively small constant. Substituting control inputs in Eq. (14), the inequalities (16) show the derivative of v is negative, such that the state trajectories will be captivated towards the sliding surfaces

Table 1
The Improved Bang-Bang Control Values for $[U_{12}(t), U_{21}(t)]$.

$N_1^T(t) \leqslant \widetilde{N}_1^{cr}(t)$, $N_2^T(t) \leqslant \widetilde{N}_2^{cr}(t)$	$N_1^T(t) \leqslant \widetilde{N}_1^{cr}(t)$, $N_2^T(t) > \widetilde{N}_2^{cr}(t)$	$N_1^T(t) > \widetilde{N}_1^{cr}(t)$, $N_2^T(t) \leqslant \widetilde{N}_2^{cr}(t)$	$N_1^T(t) > \widetilde{N}_1^{cr}(t)$, $N_2^T(t) > \widetilde{N}_2^{cr}(t)$	
$[U_{max}, U_{max}]$	$[U_{min}, U_{max}]$	$[U_{max}, U_{min}]$	If $\frac{N_1^T(t)}{\widetilde{N}_1^{jam}(t)} > \frac{N_2^T(t)}{\widetilde{N}_2^{jam}(t)}$ $[U_{max}, U_{min}]$	If $\frac{N_1^T(t)}{\widetilde{N}_1^{jam}(t)} < \frac{N_2^T(t)}{\widetilde{N}_2^{jam}(t)}$ $[U_{min}, U_{max}]$

and stay on them.

$$\begin{aligned}\dot{v}(t) \quad &\leqslant S_1(t)\rho_1(t)k_1M_{12}^X(t) - (\rho_1(t)+\beta_0)k_1M_{12}^X(t)S_1(t)\mathrm{sgn}(S_1(t)) + S_2(t)\rho_2(t)k_2M_{21}^X(t) - (\rho_2(t)+\beta_0)k_2M_{21}^X(t)S_2(t)\mathrm{sgn}(S_2(t)) \\ &\leqslant -\beta_0|S_1(t)|k_1M_{12}^X(t) - \beta_0|S_2(t)|k_2M_{21}^X(t) \leqslant 0.\end{aligned} \tag{16}$$

A bounding filter is applied to ensure the control sequences obtained from Eq. (15) are between the lower and the upper bounds (i.e. U_{min} and U_{max}). For instance, if $U_{12}(t)$ is smaller (or greater) than U_{min} (or U_{max}), then $U_{12}(t) = U_{min}$ (or $U_{12}(t) = U_{max}$) will be adopted. Note that the proposed SMC perimeter control does not necessarily require $\theta_1(t)$ and $\theta_2(t)$ values and traffic state measurements can be used. The control architecture is depicted in Fig. 2.

3.2. Improved Bang-Bang controller

To compare the performance of the proposed SMC, we consider an improved Bang-Bang (I-BB) controller. The Bang-Bang (BB) perimeter controller is a feedback control approach that aims to ensure the vehicular accumulation in a region remains under the critical value (i.e. the accumulation that generates the maximum production). The BB controller applied in the previous research (e.g. Geroliminis et al., 2013; Aalipour et al., 2018) was designed corresponding to fixed critical and jam accumulations of the region, i.e. N_I^{cr} and N_I^{jam} [veh]. The I-BB proposed here follows the same control policy yet with time-varying critical and jam accumulations,[4] i.e. $\widetilde{N}_I^{cr}(t)$ and $\widetilde{N}_I^{jam}(t)$ [veh], to capture the effect of cordon queues on the MFD.

The $\widetilde{N}_I^{cr}(t)$ is determined via the derivative of the re-scaled Production-MFD with respect to the number of traveling vehicles in Region I at time t, $\frac{\partial \widetilde{P}_I(N_I^T(t), N_{IJ}^Q(t))}{\partial N_I^T(t)} = 0$. And the re-scaled jam accumulation is considered as $\widetilde{N}_I^{jam}(t) = N_I^{jam} - N_{IJ}^Q(t)$. The I-BB controller aims to protect the more congested region by restricting the number of vehicles to enter and allowing more vehicles to leave to the less congested region. Accordingly the control values ($U_{12}(t)$ and $U_{21}(t)$) operate either at the minimum or the maximum (U_{min} or U_{max}). Detailed analytical properties of BB control policy can be referred to Aalipour et al. (2018), whereas there is a difference that the proposed I-BB uses traveling accumulations ($N_I^T(t)$) rather than total accumulations ($N_I(t)$) of Region I. The I-BB control law is summarized in Table 1.

4. Numerical experiments

In this section, the accumulation-based and trip-based MFD models and the proposed SMC perimeter control are scrutinized with two scenarios. (i) A slow-varying demand scenario to investigate the consistency between the two-region accumulation-based and trip-based MFD models considering cordon queues. This is essential because, first, the controller design and application are based on different models (i.e. accumulation-based and trip-based), second, the accumulation-based MFD model does not consider the boundary capacity and cordon queues. And (ii) a fast-varying peak-hour demand scenario to investigate the proposed SMC efficiency comparing with no control and I-BB control cases. The trip-based MFD model is applied as the plant for a typical peak-hour period in this scenario. The numerical settings under two types of demand scenarios are introduced first, and results will be analyzed and discussed in detail in the corresponding subsections. It is worth mentioning that the average trip length of each region applied in the accumulation-based MFD model is 2300 [m], and this value is the mean of the predefined distributions (as shown in Fig. 1(d)) which are employed to randomly assign trip length of each vehicle in the trip-based MFD model for both consistency check and controller performance experiments.

4.1. Models consistency and comparison

In this section, the numerical tests are adopted to investigate the characteristics and consistency between the two-region accumulation-based and trip-based MFD models. We apply the trip-based MFD model for a two-region network where each region has the same MFD with the one observed in Yokohama, Japan in Geroliminis and Daganzo (2008), as $P_I(N_I(t)) = a \cdot (N_I(t))^3 + b \cdot (N_I(t))^2 + c \cdot N_I(t)$, where $a = 9.98 \cdot 10^{-8}, b = -0.002$, and $c = 9.78$. The network schematic is shown in Fig. 1(c) with the average trip length of

[4] The performance of BB in the numerical experiment was worse than the no control case.

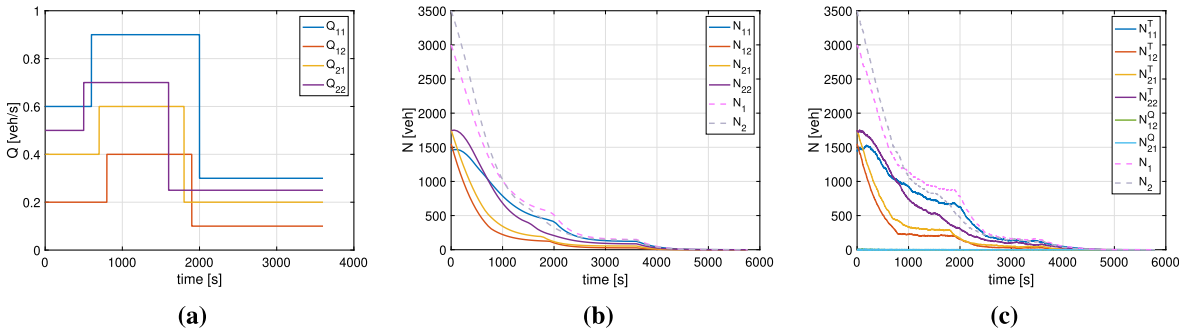

Fig. 3. (a) Slow varying two-staircase demand profile; Accumulation evolution when trip lengths follow exponential distribution: (b) accumulation-based MFD model, (c) trip-based MFD model.

2300 [m] for both regions. The boundary capacities are $\overline{C}_{12} = \overline{C}_{21} = 10$ [veh/s] and $\alpha = 0.75$. According to Lamotte and Geroliminis (2018), the two models should be equivalent when the demands vary slowly and the trip lengths are exponentially distributed, or the two models are consistent when the system reaches steady-state in spite of trip length distributions. With this in mind, we first select a slow-varying demand, as shown in Fig. 3(a), and disparate type of trip length distributions (i.e. exponential, random), for consistency check. The trip lengths are randomly selected from different distributions in an offline procedure, which are shown in Fig. 1(d). The initial accumulations in the onset of the simulation are assumed uncongested in Region 1 and congested in Region 2, where $N_1(0) =$ 3,000 [veh] and $N_2(0) =$ 3,500 [veh]. Note that the accumulation-based MFD model is FIFO and does not track cordon queue dynamics. Besides, the time step between events in the trip-based MFD model is uneven while the whole simulation period is determined by the time that the last vehicle arrives at its destination.

We check the consistency and conduct a comparison of the MFD models established in the previous section. The results are depicted in Fig. 3 and Fig. 4 with exponentially and randomly distributed trip lengths with average trip length 2300 [m]. Note that in the trip-based MFD model, each vehicle has a distinct unique trip length drawn from a distribution. For the consistency, we make sure the average trip lengths used in Eq. (8) are consistent with the mean of the distributions of the trip lengths of the vehicles. Note that the random trip lengths do not follow any specific distributions while we ensure they have the same average trip lengths as of the accumulation-based MFD model. Also note that trip lengths are not constant; each vehicle has a unique trip length in the trip-based MFD model. Fig. 3(b) and Fig. 3(c) indicate the accumulation evolution of the accumulation-based and trip-based MFD models with trip lengths following exponential distribution, while those accumulations of accumulation-based MFD model are estimated grounded on the steady-state assumption of $\theta_I(t) = N_{II}(t)/N_I(t)$ using Eq. (8). It appears that the accumulation evolution of the two MFD models are alike in trend and magnitude under the condition of slow varying demands; in accordance with the findings of Jin (2020). In Fig. 4 (a) and Fig. 4(b), accumulation exhibits discrepancies at the beginning (before 2000 [s]) while remaining constant when the system reaches steady state (after 2200 [s]). This is in accordance with Lamotte and Geroliminis (2018) which stated the two models are similar at steady-state despite how trip lengths distributed.

The accumulations in Region 1 and Region 2 in the trip-based MFD model abruptly increase when there is a large number of vehicles generated around 800 −1800 [s]. However, the accumulation-based MFD model reacts moderately with the demand surge. Since the queuing vehicles for both regions primarily leave the cordon queues at 500–600 [s], they increase the traveling accumulations in the other region. As the accumulation-based MFD does not consider the boundary capacity and cordon queues, it is expected to see it underestimates the accumulations, which is observed in Fig. 3 and Fig. 4.

Fig. 4(c) and Fig. 4(d) display the internal and external outflows of accumulation-based and trip-based MFD models with randomly selected trip lengths. The values of internal and external outflows are measured through trip-based MFD model by counting the number of vehicles which finish their trips or join the queues at each time step Δt (e.g. 2 [min]). Consequently, the sum of internal and external outflows of a region may exceed the maximum value of outflow-MFD (i.e. approximately 6.3 [veh/s]) since (i) each vehicle in the trip-based MFD model has a unique trip length which might temporarily lead to a surge in the outflow from the network. (ii) Because of the causality effect (the instantaneous change of region average speed with the change in accumulation) in transition periods the observed outflows are higher. (iii) Lastly, the queuing process at the regions boundary adds inherent delays in external outflows which propagates in accumulations and internal outflows.

The evolution of $\theta(t)$ of the two MFD models are depicted in Fig. 4(e) and Fig. 4(f). In accumulation-based MFD model, $\theta_I(t)$ is continuous in time and instantaneous and is estimated as $N_{II}(t)/N_I(t)$. Yet it appears that this estimation is not always accurate. As in Fig. 4(e), $\theta_I(t)$ should be very close to one at the end of the studied period as a result of extra time needed for transferred vehicles to finish their trips. Unlike the estimation of $\theta_I(t)$ in accumulation-based MFD model, we consider to obtain it via outflows in the trip-based MFD model, i.e. $\theta_I(t) = M_{II}(t)/(M_{II}(t) + M_{IJ}(t))$. Note that considering $N_{IJ}(t)/N_I(t)$ equals to $\theta_I(t)$ might be reliable under several conditions, e.g. exponential distributed trip lengths and steady state conditions, whereas it is less accurate under time-varying and complex situations. Thus a robust controller with respect to $\theta(t)$ uncertainty (which is a byproduct of cordon queues and heterogeneous distributions of destinations) is needed.

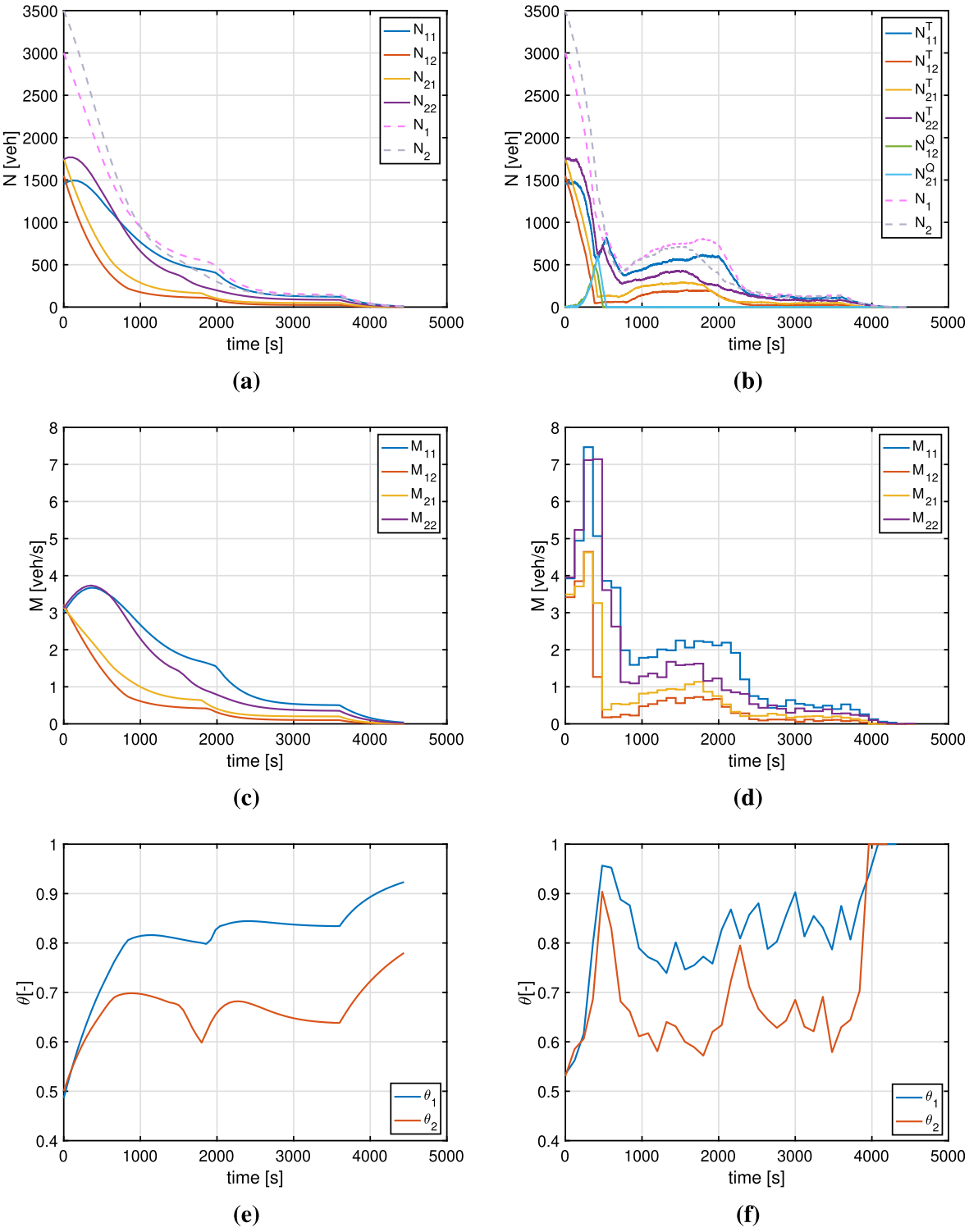

Fig. 4. Accumulation evolution when trip lengths are randomly distributed: (a) accumulation-based MFD model, (b) trip-based MFD model; Evolution of internal and external flows: (c) accumulation-based MFD model, (d) trip-based MFD model; Evolution of $\theta(t)$: (e) accumulation-based MFD model, (f) trip-based MFD model.

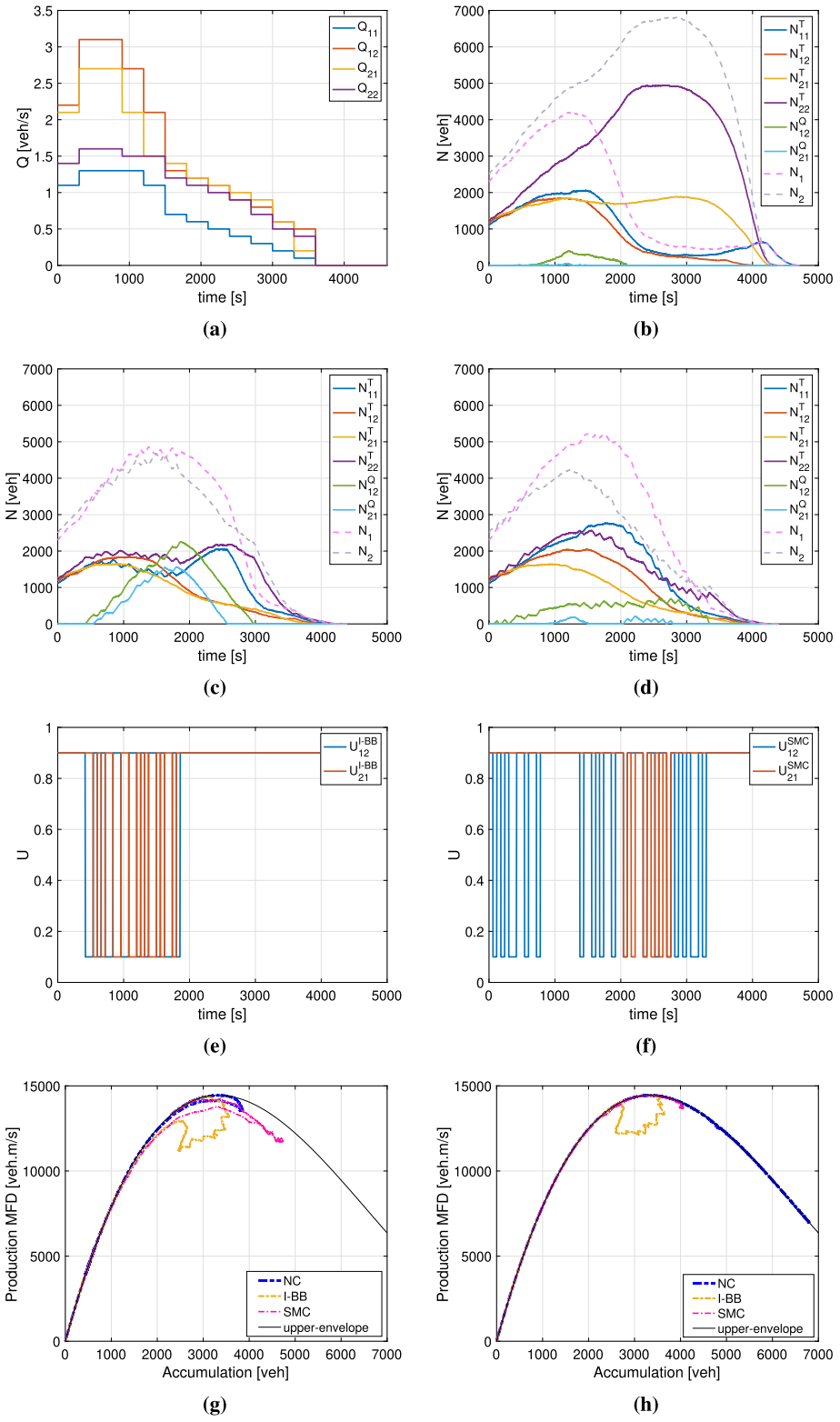

Fig. 5. (a) Peak-hour demands; Accumulation evolution: (b) no control, (c) improved bang-bang control, (d) proposed sliding mode control; Perimeter control actions: (e) improved bang-bang control, (f) proposed sliding mode control; (g) Production-MFD of Region 1, (h) Production-MFD of Region 2. The hysteresis loop in MFDs and the drop in average region speed are consequences of cordon queues. Note that the controllers update interval is 60 s.

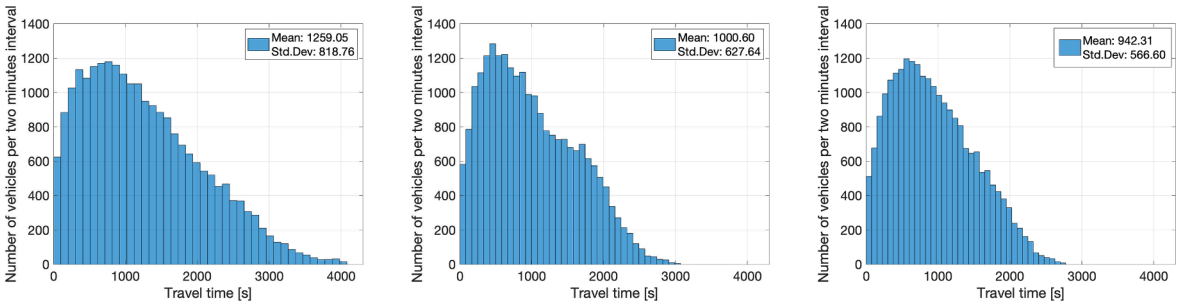

Fig. 6. The histogram of vehicles' travel times under three control methods (23202 vehicles in total): (a) no control; (b) I-BB control, and (c) the proposed SMC. Note that the controllers update interval is 60 s.

4.2. Controller performance

In this section, a scenario with typical peak-hour travel demands is presented to explore the performance of the proposed SMC perimeter controller. The two-region trip-based MFD model considering cordon queues is employed as the plant. In this scenario, the network is initially in uncongested conditions for both regions with initial accumulations of $N_1(0) = 2{,}300$ [veh] and $N_2(0) = 2{,}500$ [veh] respectively. Note that the accumulation-based and trip-based MFD models rely on the same MFD functions but with different representations, i.e. Production-MFD and Speed-MFD. Perimeter control values are calculated using I-BB and SMC with the lower bound as $U_{\min} = 0.1$ and the upper bound as $U_{\max} = 0.9$. Both controllers change the perimeter control values every minute. In the no control case, $U_{12}(t) = U_{21}(t) = U_{\max}$ are applied over the studied time duration. Furthermore, the parameters in sliding surface are selected as $k_1 = 2$ and $k_2 = 4$. Considering the upper-envelope MFD, the region critical and jam accumulations are 3,334 and 10,000 [veh], respectively. However, the re-scaled MFD alters the critical and jam accumulations, i.e. $\widetilde{N}_I^{\mathrm{cr}}(t)$ and $\widetilde{N}_I^{\mathrm{jam}}(t)$, over time such that the two accumulations will be adjusted in every iteration under I-BB control framework.

Three scenarios are compared to examine the proposed controller efficiency: 1) no perimeter control, 2) I-BB perimeter control, and 3) SMC. We take the no control case as the base scenario and apply the I-BB control for comparison. The I-BB perimeter control is a state feedback control method considering the current number of traveling vehicles in the regions (i.e. $N_I^{\mathrm{T}}(t)$) and comparing it with re-scaled time-varying critical and jam accumulations in order to protect the more congested region. A fast varying rush-hour demand profile is employed, as shown in Fig. 5(a). The network faces increasing traffic demands before 900 [s], while the demands gradually drop to zero to ensure the clearance of the network at the end of the simulation. The accumulation evolution over studied period of trip-based MFD model corresponding to no control, I-BB control, and SMC are depicted in Fig. 5(b)-(d) respectively. With the absence of control, the control sequences always operate at the maximum such that a few queued vehicles (i.e. $N_{12}^{\mathrm{Q}}(t) < 500$ [veh]) are detected and the cordon queues dissipate promptly, as shown in Fig. 5(b). Also, Region 2 is the more congested one and requires protection in the no control case. It can be observed that the accumulation difference between the two regions shrinks when either I-BB or SMC is employed, whereas both controllers lead to additional vehicles queuing at the cordons compare with the no control case. The control sequences of I-BB and SMC controllers are depicted in Fig. 5(e) and Fig. 5(f). Note that before 500 [s], there are no queued vehicles in I-BB control case because both $U_{12}(t)$ and $U_{21}(t)$ are the maximum value, but they are observed in SMC case since the perimeter control is active from the beginning to restrict the vehicles passing the boundary between Region 1 and 2. Afterwards, between 500–1800 [s], the perimeter control oscillates either at the maximum or the minimum values of the I-BB control case. The chattering behavior of control sequences is evident as I-BB tries to proportionally equalize the accumulations of both regions. In contrast, the SMC protects the more congested Region 2. As shown in Fig. 5(f), $U_{21}(t)$ operates at $U_{\max}$ between 0 and 2100 [s] while $U_{12}(t)$ is chattering to limit the vehicles in Region 1 to enter Region 2.

Perimeter control is a way to distribute vehicles more uniformly in the network yet could ease the network congestion to some extent. The number of cordon queued vehicles in both regions are higher in I-BB control case compare to no control and SMC, such that more vehicles suffer queuing delays because of the perimeter control. The cordon queues in Region 1 and Region 2, $N_{12}^{\mathrm{Q}}(t)$ and $N_{21}^{\mathrm{Q}}(t)$, are continuously expanding and concentrating at the cordons from 500 [s] to 1800 [s] with the peak values of 2255 [veh] and 1558 [veh] respectively. The vehicles queued near cordons reduces the average speed of traveling vehicles. However, the number of queuing vehicles corresponding to SMC is much smaller than I-BB control case. With SMC, the cordon queues are long-lived (appear sooner and diminish later) and moderate, which helps curb the negative effect of cordon queues on the speed of traveling vehicles. Furthermore, SMC results in chattering perimeter control actions that reduce the maximum size of cordon queues, with the peak value of 693 [veh] in SMC and 2255 [veh] in I-BB. Note that the control values of SMC are oscillating between $U_{\min}$ and $U_{\max}$ since the controllers are incorporated with a limiting filter. No perimeter control values are observed in between as a consequence of the magnitude of sliding surface parameters, i.e. k_1 and k_2. Higher parameters can be applied whereas the controller performance might be deteriorated.

It assuredly alleviates the congestion in Region 2 when either controller applies; the maximum accumulation reduces from 6790 [veh] with no control to 4658 [veh] with I-BB control and 4207 [veh] with the proposed SMC. This comes at an expense of more vehicles in Region 1; the maximum accumulation extends from 4188 [veh] with no control to 4834 [veh] with I-BB control and 5198

Table 2
Network-level statistics (averaged over 10 runs) for the three scenarios. The numbers in parenthesis indicate the improvement in performance compare with the no control case. Cycle time denotes the controller updating intervals.

Scenario	Cycle time [s]	Total Time Spent [veh·s]	Average Travel Time [s/veh]
No Control		2.6598×10^7	1178.4
I-BB	60	2.1460×10^7 (−19.3%)	950.7
SMC	60	2.0682×10^7 (−22.3%)	916.3
I-BB	120	2.1475×10^7 (−19.3%)	951.4
SMC	120	2.0711×10^7 (−22.1%)	917.6

[veh] with SMC. One observation worth mentioning is in the no control case, Region 2 is the more congested one that needs protection, but this order switches (Region 1 becomes more congested) in the SMC case.

Fig. 5(g) and Fig. 5(h) depicts the Production-MFD of Region 1 and Region 2 for all control cases where hysteresis loops are observed. Previous research (e.g. Mahmassani et al., 2013) suggested that the clockwise hysteresis loops are more likely to happen as a consequence of the heterogeneity of congestion distribution in a region. In this paper, the trip-based MFD model considers the impact of cordon queues, therefore the congestion is not uniformly distributed especially with considerable cordon queues or with protracted time for queue dissipation. Results indicate that SMC leads to a more homogeneous network as the Production-MFDs for both regions display negligible hysteresis loops and the accumulation difference between regions is insignificant. The Production-MFD in the trip-based MFD model is the re-scaled one, therefore it can be observed that the Production-MFD curves are lower than the upper-envelope Production-MFD.

Comparing the three control cases, (see Fig. 5, Fig. 6, and Table 2), we notice the advantages of SMC compared to the I-BB controller. The objective of the SMC is minimizing the total time spent that is equivalent to minimize the total number of vehicles in the network. Table 2 lists the average travel time [s/veh] and total time spent [veh·s] of I-BB perimeter control, the proposed SMC cases along with the no control case. The controller updating cycle times are 60 and 120 s, respectively. Tabulated values are obtained through the average results out of ten simulations. The values in parentheses are the change in the percentage of total network performance compare with the no control case. With a limited number of switching control efforts, the total travel time spent in the network with I-BB control is decreased 19.3% on average, whereas the network performance is improved 22.3% by the proposed SMC. Additionally, the outcomes indicate that the average travel time is reduced with both controllers while SMC performs superior to I-BB.

Fig. 6 shows the histogram of the vehicles' travel times under no control, I-BB, and the proposed SMC perimeter control. The distribution of travel times for the three control cases has an overall skewed-right shape. Specifically, the range of travel times under each control case is different, with a wider range of no control (i.e. 0 to 4078 [s]) yet concentrated under both I-BB control (i.e. 0 to 3039 [s]) and SMC (i.e. 0 to 2751 [s]). Besides, the travel time under SMC shows a relatively small variation with standard deviation equals to 567 [s] compare to 819 [s] of no control and 628 of I-BB control cases (see in Fig. 6). Therefore, a more fair travel time distribution and a more uniform congestion distribution are obtained with perimeter control based on the proposed SMC.

5. Summary and future work

This paper has developed a real-time, robust perimeter controller building on the SMC concept to address modeling uncertainty associated with internal and external outflow estimations in accumulation-based MFD models. The proposed controller can tackle the cordon queues (i.e. vehicles concentrated at boundaries waiting to enter the other regions), which are the byproduct of perimeter control. Cordon queues may intensify local impediments on traveling vehicles (e.g. occupy road space and reduce region speed) and affect internal and external outflows. A two-region trip-based MFD model is proposed as the plant involving cordon queue dynamics to investigate the effectiveness of the proposed control strategy. An improved Bang-Bang perimeter controller is introduced for comparison.

Since the proposed controller is constructed and utilized on two different models, it is vital to scrutinize the consistency and bear comparison between them. The accumulation-based MFD model neglects cordon queues to simplify the controller design. Besides, unlike the trip-based MFD model, the accumulation-based MFD does not track individual vehicles and does not consider vehicles' trip lengths and departure times. Numerical tests showed that SMC is fairer with reducing the spread of vehicles' travel times. Also, there is a considerable improvement in network performance since the proposed SMC helps to evenly distribute the accumulations in the network and reduce the total time spent around 22.3% compare to the no control case. In comparison, the I-BB control likewise improved the network efficiency of approximately 19.3% yet with excessive queuing vehicles in both regions that lead to concentrated congestion near the cordon. Consequently, SMC results in a more homogeneous network as the hysteresis loops are reduced in Production-MFDs compared to I-BB. Both SMC and I-BB belong to variable structure control methods that are discontinuous in nature and accordingly versatile. Aalipour et al. (2018) showed that BB is the optimal perimeter control (corroborated in Ni and Cassidy (2020)). The main challenge of I-BB is the switching procedure (when the perimeter control gain should switch between $U_{\min}$ and $U_{\max}$. The proposed SMC enables this with a systematic and measurement-based formulation.

In future works, the robust controller should address networks with multiple modes of transport. Another future research is to extend the network structure to include multiple regions with multiple paths and trip lengths that require modeling regional route choice. A challenge would be to incorporate the effect of queued vehicles at the regions' boundaries into the route choice of vehicles in

the trip-based MFD model. The effect of perimeter control on the departure time choice can also shed light on practical complications of field implementation. Moreover, investigating an integration of SMC with other optimal and/or proactive controllers (e.g. MPC) is a priority research direction. Investigating a time-varying cordon location could alleviate the local impacts of cordon queues. This is a promising future research direction.

CRediT authorship contribution statement

Ye Li: Methodology, Software, Validation, Formal analysis, Investigation, Data curation, Writing - original draft, Writing - review & editing. **Mehmet Yildirimoglu:** Methodology, Formal analysis, Investigation, Writing - review & editing. **Mohsen Ramezani:** Conceptualization, Methodology, Validation, Formal analysis, Investigation, Writing - original draft, Writing - review & editing, Supervision.

References

Aalipour, A., Kebriaei, H., Ramezani, M., 2017. Nonlinear robust traffic flow control in urban networks. IFAC-PapersOnLine 50 (1), 8537–8542.
Aalipour, A., Kebriaei, H., Ramezani, M., 2018. Analytical optimal solution of perimeter traffic flow control based on mfd dynamics: a pontryagin's maximum principle approach. IEEE Trans. Intell. Transp. Syst. 20 (9), 3224–3234.
Amirgholy, M., Nourinejad, M., Gao, H.O., 2020. Optimal traffic control at smart intersections: Automated network fundamental diagram. Transp. Res. Part B: Methodol. 137, 2–18.
Arnott, R., 2013. A bathtub model of downtown traffic congestion. J. Urban Econ. 76, 110–121.
Batista, S.F., Leclercq, L., 2019. Regional dynamic traffic assignment framework for macroscopic fundamental diagram multi-regions models. Transp. Sci. 53 (6), 1563–1590.
Bichiou, Y., Elouni, M., Abdelghaffar, H.M., Rakha, H.A., 2020. Sliding mode network perimeter control. IEEE Trans. Intell. Transp. Syst.
Canale, M., Fagiano, L., Ferrara, A., Vecchio, C., 2008. Comparing internal model control and sliding-mode approaches for vehicle yaw control. IEEE Trans. Intell. Transp. Syst. 10 (1), 31–41.
Csikós, A., Charalambous, T., Farhadi, H., Kulcsár, B., Wymeersch, H., 2017. Network traffic flow optimization under performance constraints. Transp. Res. Part C: Emerg. Technol. 83, 120–133.
Daganzo, C.F., 2007. Urban gridlock: Macroscopic modeling and mitigation approaches. Transp. Res. Part B: Methodol. 41 (1), 49–62.
Fu, H., Liu, N., Hu, G., 2017. Hierarchical perimeter control with guaranteed stability for dynamically coupled heterogeneous urban traffic. Transp. Res. Part C: Emerg. Technol. 83, 18–38.
Fu, Y., Li, S., Yang, L., 2020. Robust perimeter control design for two urban regions with sampled-data and input saturation. Transportmetrica B: Transp. Dyn. 1–23.
Geroliminis, N., Daganzo, C.F., 2008. Existence of urban-scale macroscopic fundamental diagrams: Some experimental findings. Transp. Res. Part B: Methodol. 42 (9), 759–770.
Geroliminis, N., Haddad, J., Ramezani, M., 2013. Optimal perimeter control for two urban regions with macroscopic fundamental diagrams: a model predictive approach. IEEE Trans. Intell. Transp. Syst. 348–359.
Godfrey, J., 1969. The mechanism of a road network. Traffic Eng. Control 8 (8).
Haddad, J., 2015. Robust constrained control of uncertain macroscopic fundamental diagram networks. Transp. Res. Part C: Emerg. Technol. 59, 323–339.
Haddad, J., 2017. Optimal perimeter control synthesis for two urban regions with aggregate boundary queue dynamics. Transp. Res. Part B: Methodol. 96, 1–25.
Haddad, J., Mirkin, B., 2020. Resilient perimeter control of macroscopic fundamental diagram networks under cyberattacks. Transp. Res. Part B: Methodol. 132, 44–59.
Haddad, J., Shraiber, A., 2014. Robust perimeter control design for an urban region. Transp. Res. Part B: Methodol. 68, 315–332.
Han, Y., Ramezani, M., Hegyi, A., Yuan, Y., Hoogendoorn, S., 2020. Hierarchical ramp metering in freeways: an aggregated modeling and control approach. Transp. Res. Part C: Emerg. Technol. 110, 1–19.
Huang, Y., Xiong, J., Sumalee, A., Zheng, N., Lam, W., He, Z., Zhong, R., 2020. A dynamic user equilibrium model for multi-region macroscopic fundamental diagram systems with time-varying delays. Transp. Res. Part B: Methodol. 131, 1–25.
Ingole, D., Mariotte, G., Leclercq, L., 2020. Perimeter gating control and citywide dynamic user equilibrium: A macroscopic modeling framework. Transp. Res. Part C: Emerg. Technol. 111, 22–49.
Jin, W.-L., 2020. Generalized bathtub model of network trip flows. Transp. Res. Part B: Methodol. 136, 138–157.
Keyvan-Ekbatani, M., Kouvelas, A., Papamichail, I., Papageorgiou, M., 2012. Exploiting the fundamental diagram of urban networks for feedback-based gating. Transp. Res. Part B: Methodol. 46 (10), 1393–1403.
Keyvan-Ekbatani, M., Papageorgiou, M., Knoop, V.L., 2015. Controller design for gating traffic control in presence of time-delay in urban road networks. Transp. Res. Part C: Emerg. Technol. 59, 308–322.
Kim, S., Tak, S., Lee, D., Yeo, H., 2019. Distributed model predictive approach for large-scale road network perimeter control. Transp. Res. Rec. 2673 (5), 515–527.
Kouvelas, A., Saeedmanesh, M., Geroliminis, N., 2017. Enhancing model-based feedback perimeter control with data-driven online adaptive optimization. Transp. Res. Part B: Methodol. 96, 26–45.
Lamotte, R., Geroliminis, N., 2018. The morning commute in urban areas with heterogeneous trip lengths. Transp. Res. Part B: Methodol. 117, 794–810.
Lei, T., Hou, Z., Ren, Y., 2019. Data-driven model free adaptive perimeter control for multi-region urban traffic networks with route choice. IEEE Trans. Intell. Transp. Syst.
Loder, A., Dakic, I., Bressan, L., Ambühl, L., Bliemer, M.C., Menendez, M., Axhausen, K.W., 2019. Capturing network properties with a functional form for the multi-modal macroscopic fundamental diagram. Transp. Res. Part B: Methodol. 129, 1–19.
Mahmassani, H.S., Saberi, M., Zockaie, A., 2013. Urban network gridlock: Theory, characteristics, and dynamics. Transp. Res. Part C: Emerg. Technol. 36, 480–497.
Mariotte, G., Leclercq, L., 2019. Flow exchanges in multi-reservoir systems with spillbacks. Transp. Res. Part B: Methodol. 122, 327–349.
Mariotte, G., Leclercq, L., Batista, S., Krug, J., Paipuri, M., 2020a. Calibration and validation of multi-reservoir mfd models: A case study in lyon. Transp. Res. Part B: Methodol. 136, 62–86.
Mariotte, G., Leclercq, L., Laval, J.A., 2017. Macroscopic urban dynamics: Analytical and numerical comparisons of existing models. Transp. Res. Part B: Methodol. 101, 245–267.
Mariotte, G., Paipuri, M., Leclercq, L., 2020b. Dynamics of flow merging and diverging in mfd-based systems: Validation vs. microsimulation. Front. Future Transp. 1, 3.
Mohajerpoor, R., Saberi, M., Vu, H.L., Garoni, T.M., Ramezani, M., 2019. H_∞ robust perimeter flow control in urban networks with partial information feedback. Transp. Res. Part B: Methodol.
Ni, W., Cassidy, M., 2020. City-wide traffic control: modeling impacts of cordon queues. Transp. Res. Part C: Emerg. Technol.
Paipuri, M., Leclercq, L., 2020. Bi-modal macroscopic traffic dynamics in a single region. Transp. Res. Part B: Methodol. 133, 257–290.
Ramezani, M., Haddad, J., Geroliminis, N., 2015. Dynamics of heterogeneity in urban networks: aggregated traffic modeling and hierarchical control. Transp. Res. Part B: Methodol. 74, 1–19.

Ramezani, M., Nourinejad, M., 2018. Dynamic modeling and control of taxi services in large-scale urban networks: A macroscopic approach. Transp. Res. Part C: Emerg. Technol. 94, 203–219.
Saedi, R., Saeedmanesh, M., Zockaie, A., Saberi, M., Geroliminis, N., Mahmassani, H.S., 2020. Estimating network travel time reliability with network partitioning. Transp. Res. Part C: Emerg. Technol. 112, 46–61.
Saeedmanesh, M., Geroliminis, N., 2016. Clustering of heterogeneous networks with directional flows based on "snake" similarities. Transp. Res. Part B: Methodol. 91, 250–269.
Sirmatel, I.I., Geroliminis, N., 2019. Nonlinear moving horizon estimation for large-scale urban road networks. IEEE Trans. Intell. Transp. Syst.
Slotine, J.-J.E., 1984. Sliding controller design for non-linear systems. Int. J. Control 40 (2), 421–434.
Spurgeon, S., 2014. Sliding mode control: a tutorial. In: 2014 European Control Conference (ECC). IEEE, pp. 2272–2277.
Yang, K., Menendez, M., Zheng, N., 2019. Heterogeneity aware urban traffic control in a connected vehicle environment: A joint framework for congestion pricing and perimeter control. Transp. Res. Part C: Emerg. Technol. 105, 439–455.
Yang, K., Zheng, N., Menendez, M., 2018. Multi-scale perimeter control approach in a connected-vehicle environment. Transp. Res. Part C: Emerg. Technol. 94, 32–49.
Yildirimoglu, M., Ramezani, M., 2020. Demand management with limited cooperation among travellers: a doubly dynamic approach. Transp. Res. Part B: Methodol.
Yildirimoglu, M., Ramezani, M., Geroliminis, N., 2015. Equilibrium analysis and route guidance in large-scale networks with mfd dynamics. Transp. Res. Part C: Emerg. Technol. 59, 404–420.
Yildirimoglu, M., Sirmatel, I.I., Geroliminis, N., 2018. Hierarchical control of heterogeneous large-scale urban road networks via path assignment and regional route guidance. Transp. Res. Part B: Methodol. 118, 106–123.
Zheng, N., Geroliminis, N., 2020. Area-based equitable pricing strategies for multimodal urban networks with heterogeneous users. Transp. Res. Part A: Policy Pract. 136, 357–374.
Zhong, R., Chen, C., Huang, Y., Sumalee, A., Lam, W., Xu, D., 2018. Robust perimeter control for two urban regions with macroscopic fundamental diagrams: A control-Lyapunov function approach. Transp. Res. Part B: Methodol. 117, 687–707.